

New Eh-pH (Pourbaix) diagrams of the copper-tin system

W. Thomas Chase^{a*}, Michael Notis^b and Arthur D. Pelton^c

^a Chase Art Services, 508 route 169, Woodstock, Connecticut 06281, USA

^b Lehigh University Department of Materials Science and Engineering, Whitaker Laboratory #5, Bethlehem, PA 18015, USA

^c Centre de Recherche en Calcul Thermochimique, Department. Of Chemical Engineering, Ecole Polytechnique, P. O. Box 6079, Station "Downtown" Montreal, Quebec H3C 3A7, Canada

* Corresponding author: TChase4921@aol.com

Abstract

New versions of the conventional Eh-pH or Pourbaix diagrams, incorporating copper and tin together as well as intermetallic phases, yield an enhanced understanding of corrosion processes. The diagrams clarify the corrosion possibilities for bronzes in different environments, emphasize the role of tin oxide in bronze corrosion, and point toward possibilities for future research

Keywords: Eh-pH diagrams, Pourbaix, copper, tin, corrosion, tin oxide, redeposited copper, burial, environment

Introduction

Enhanced understanding of corrosion during exposure, burial, or submersion can help predict the condition of archaeological bronzes and enable us to say something about their environments. These studies may help in grouping bronzes from unknown provenances and in differentiating naturally corroded bronzes from those which have been patinated artificially. Improved understanding of corrosion also aids conservation

assessments and treatments. Eh-pH or Pourbaix diagrams have been a very useful tool in understanding corrosion. To date, these have been drawn using data for pure metals. Inclusion of both copper and tin on the same diagram helps to elucidate corrosion processes.

History of Pourbaix diagrams in conservation studies

The study of bronze corrosion has a very long history (Scott

Table 1: System Cu-Sn-Cl-H₂O

Pelton Figure No.	Our Figure No.	m (Cl ⁻) mol/kgH ₂ O	m(aqueous species) mol/kgH ₂ O	Comments
1		10 ⁻³ (35 ppm)	1.0	
2		"	10 ⁻³	
3		"	10 ⁻⁶	
4	5.7	10 ⁻² (355 ppm)	1.0	
4a		"	1.0	CuCl ₃ ⁻ (aq) included
4b		"	1.0	Cu(OH) ₂ (s) included
4c	4A	"	1.0	With metastable Cu ₄ Sn
4d	4B	"	1.0	With no intermetallics Cu ₄ Sn _n
4e		"	1.0	T = 313.15 K
5		"	10 ⁻³	
6		"	10 ⁻⁶	
7		10 ⁻¹ (3550 ppm)	1.0	
8		"	10 ⁻³	
9		"	10 ⁻⁶	
10		1.0 (35500 ppm)	1.0	
10a		"	1.0	
11		"	10 ⁻³	
12		"	10 ⁻⁶	

Table 2: System Cu-Sn-CO₂-H₂O

Pelton Figure No.	Our Figure No.	m(CO ₂) mol/kgH ₂ O	m(aqueous species) mol/kgH ₂ O	Comments
13	2	10 ⁻³ (44 ppm)	1.0	
14		"	10 ⁻³	
15		"	10 ⁻⁶	
16	2	10 ⁻² (440 ppm)	1.0	
17		"	10 ⁻³	
18	3	"	10 ⁻⁶	
19	2	10 ⁻¹ (4400 ppm)	1.0	
20		"	10 ⁻³	
21		"	10 ⁻⁶	
22	2, 4, 5, and 7	1.0 (44000 ppm)	1.0	
22a		"	1.0	NBS data
22b		"	1.0	NBS data including Cu(OH) ₂ (s)
22c		"	1.0	T = 313.15 K
23		"	10 ⁻³	
24		"	10 ⁻⁶	

2002). In 1976, at a meeting on corrosion and metal artifacts at the U. S. National Bureau of Standards (now NIST), Marcel Pourbaix delivered a useful tutorial stressing Eh-pH diagrams (Pourbaix 1977). Since then, Pourbaix diagrams have frequently been used in explaining corrosion of historic bronzes (Schweizer 1994; Lins and Power 1994; Scott 2002; etc.).

FactSage software

In the 1970's computerized software for calculating Eh-pH diagrams became available. One of the most widely used programs is FactSage, which originated from the F*A*C*T program (Facility for the Analysis of Chemical Thermodynamics; Pelton et al. 1977; Bale et al. 2002; www.factsage.com). Dr. Notis suggested to Wang Dongning, a doctoral candidate at Lehigh University, that she uses the F*A*C*T program to prepare Pourbaix diagrams of the Cu-Sn-H₂O system with and without the thermodynamic data for the epsilon-Cu₃Sn phase. The diagrams showed enlarged areas of stability for copper, cuprite (Cu₂O), and tenorite (CuO) (Wang 1997). Epsilon-Cu₃Sn appears as a separate phase, stable below the lower limit of stability of water.

New diagrams

In subsequent discussions, Chase and Notis decided that it would be worthwhile to pursue construction of Eh-pH diagrams for Cu, Sn and their intermetallics at various conditions which one might encounter in archaeology. Pelton was engaged as a collaborator, and he produced a report with 33 Eh-pH diagrams. The full report is available on the Lehigh University Archaeometallurgy Program website, <http://www.lehigh.edu/~inarcmet>. Diagrams were calculated for various concentrations of chloride ion (see table 1) or total dissolved CO₂ (see table 2), and for concentrations of other aqueous species of 1.0, 10⁻³ and 10⁻⁶ molal (mol/kg H₂O), using FactSage software. Sources for data for the various species are available in Pelton's report. Selected diagrams are reproduced here (see figures 1-4).

SnO₂ – prevalence of tin dioxide

Solid SnO₂ is the stable Sn-containing phase everywhere between the P_{O₂} = 1 and P_{H₂} = 1 lines in all figures except in a couple of cases at very low pH and under very reducing conditions. While this was clearly visible in Wang Dongning's figures, its importance became evident only after Pelton's report.

Tin is present in metallic form in the compound Cu₃Sn(s) [epsilon-iron] only below the P_{H₂} = 1 line (see figure 1, at bottom). When the diagrams were redrawn using the metastable Cu₄Sn(s) (corresponding to delta) the same condition prevailed (see figure 3A). Redrawing them using only copper and tin without intermetallics showed a decreased stability for tin (see figure 3B). Tin oxide is very insoluble. It should not be a surprise to encounter it almost anywhere on corroded bronzes.

Concentration effects in the Cu-Sn-CO₂-H₂O system

A combined diagram of the Cu-Sn-CO₂-H₂O system at various concentrations of CO₂ and molality of 1 for other dissolved species is shown as figure 1. The upper limit of the range of concentrations of CO₂ (log₁₀ m(CO₂) = 0, or 4.4%) corresponds to the lowest value cited for the Tienma-Qucun site by Wang (2002, p44), where CO₂ concentrations range up to 8.2%. At these concentrations, the right-hand limit of the field of stability of malachite is displaced toward higher pH, and the field of stability of tenorite, a corrosion product rarely seen on excavated bronzes, becomes smaller. Incidentally, the question of stability of malachite or azurite seems to be moot. Pelton's examination of the thermodynamic data showed that these two solids have very similar stabilities and, within the error limits of the data, one or the other, or both, could be stable.

Comparing figure 1 with a diagram where the concentration of dissolved species is much lower (see figure 2, log₁₀ m(CO₂) = -2, molality of 10⁻⁶ for other dissolved species) shows that the area where copper will dissolve (Cu²⁺ + SnO₂(s)) is much larger. It ranges downward to pH 6.5 and Eh +0.175mV. This is well within outdoor conditions in rain. Copper will dissolve and tin will form SnO₂(s). On outdoor bronzes, especially bells with large grains, the alpha centers of the dendrites can be seen to

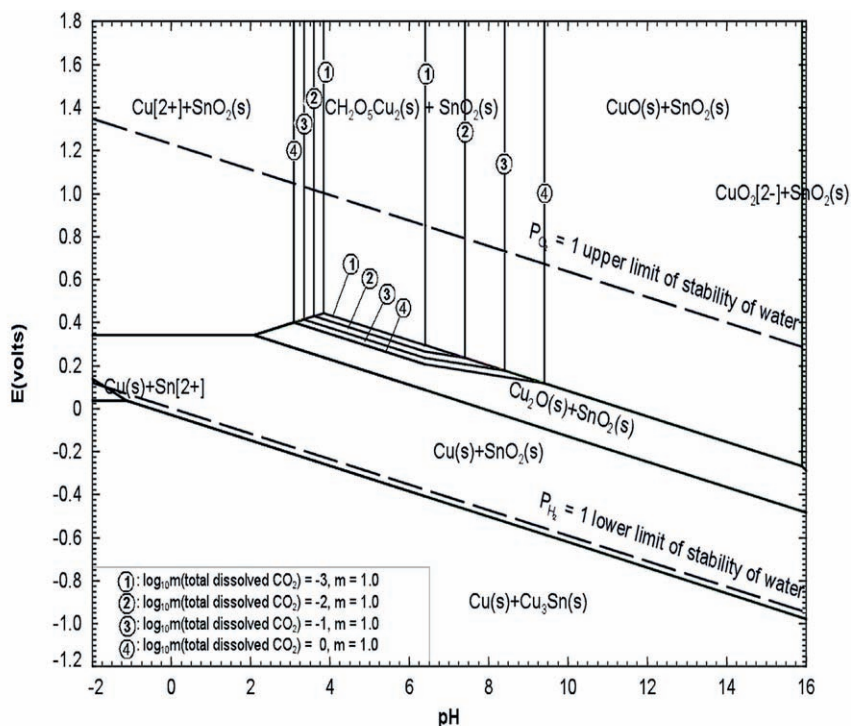


Figure 1: Eh-pH diagram for the Cu-Sn-CO₂-H₂O system at 298.15°K. Log₁₀ m(CO₂) = -3 to 0 (44 ppm to 4.4%); log₁₀ m for other aqueous species = 1. Different concentrations of CO₂ are marked by circled numbers

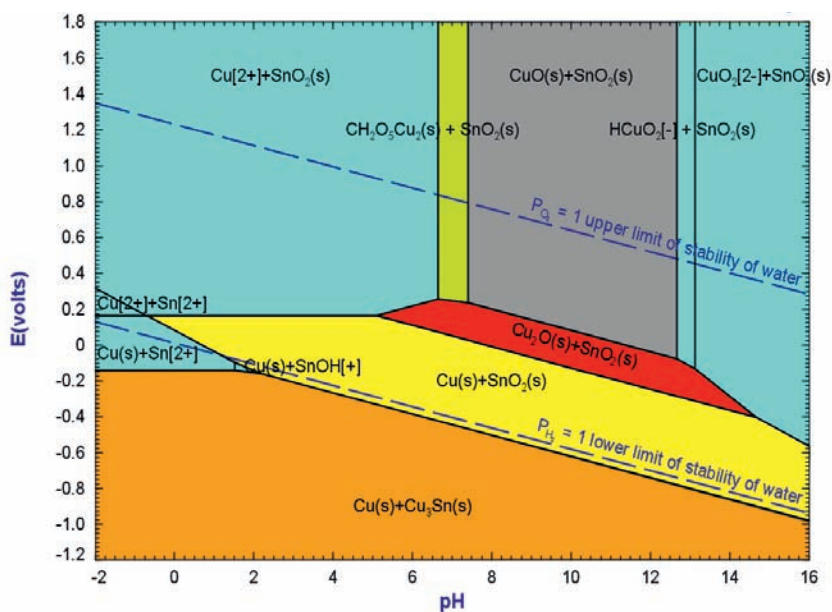


Figure 2: Eh-pH diagram for the Cu-Sn-CO₂-H₂O system at 298.15°K. Log₁₀ m(CO₂) = -2 (440 ppm); log₁₀ m for other aqueous species = -6. Note the increased solubility of copper at the upper left

have corroded, and the delta is still silvery and shiny – probably protected by SnO₂.

The Cu-Sn-Cl-H₂O system

Figures 3A and 3B show the Cu-Sn-Cl-H₂O system at log₁₀ m(Cl⁻) = -2 (355 ppm) and a molality of 1 for other dissolved species. The usual array of areas of stability for the copper minerals is seen here; each contains SnO₂(s). At lower concentrations of chloride and other dissolved species than are shown here, dissolution takes place more rapidly, and the fields of stability of nantokite (CuCl) and paratacamite (Cu₄(OH)₆Cl₂) disappear. At log₁₀ m(Cl⁻) = -3 (35 ppm), these fields are present

when the molality of other dissolved species is 1.0, but absent when it is 10⁻³.

A combined diagram including both Cl⁻ and CO₂

FactSage software cannot yet calculate diagrams when Cl⁻ and dissolved CO₂ are present simultaneously. The diagrams can, however, be combined manually (see figure 4; details in Pelton's report). Here the conditions are as follows: log₁₀ m(Cl⁻) = -2 (355 ppm); log₁₀ m(CO₂) = 0 (4.4%); a molality of 1 for other dissolved species – conditions similar to stagnant groundwater in a deep tomb in the loess area of China. There is enough Cl⁻ so that nantokite (CuCl) can form, although only in fairly acidic conditions.

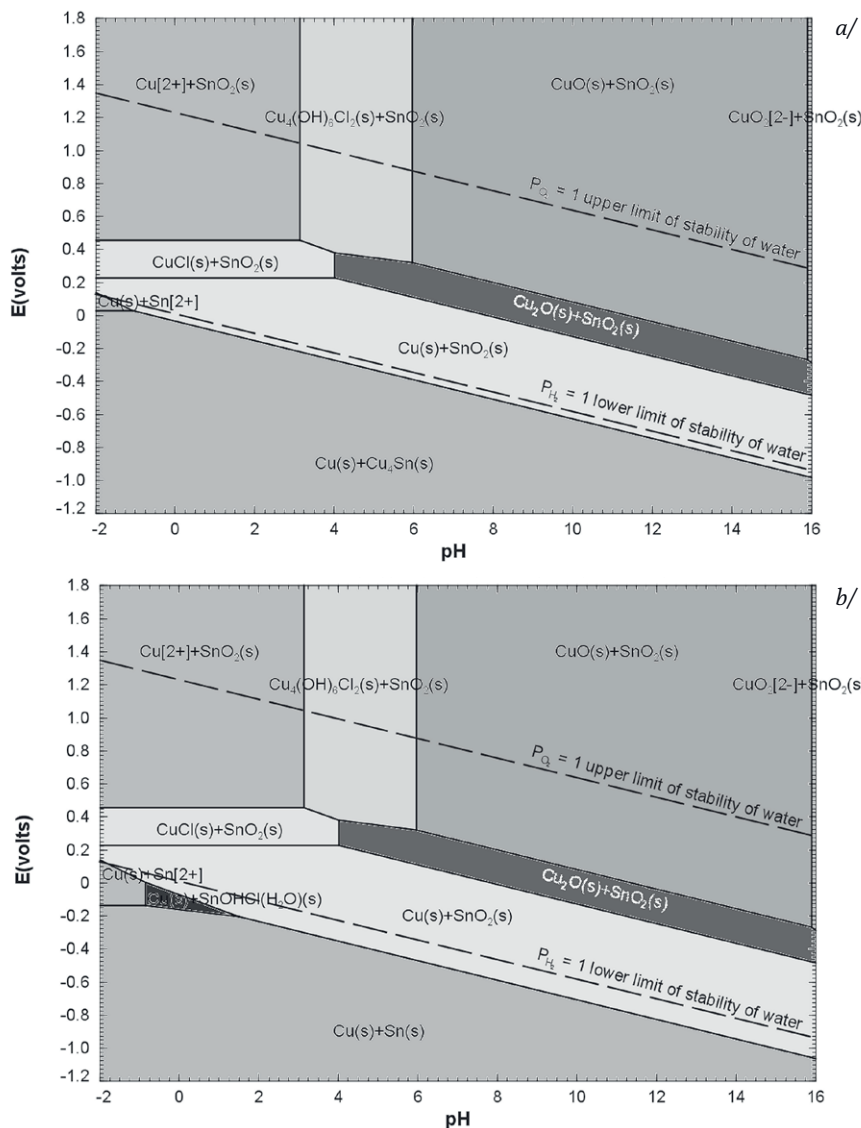


Figure 3: Two Eh-pH diagrams for the Cu-Sn-Cl-H₂O system at 298.15°K. Log₁₀ m(Cl⁻) = -2 (355 ppm) ; log₁₀ m for other aqueous species = 1. Figure 3a was drawn using Cu and metastable Cu₄Sn (δ). Figure 3b was drawn using pure Cu and Sn. Note the difference in position of the upper limit for stability of both metallic phases together just below the lower limit of stability of water.

Terrestrial (and marine) environments are shown in figure 5. The thin line around the point cloud shows the limits of possible environments at atmospheric pressure.

Superimposing the point cloud on the Eh-pH diagram of figure 4 produces figure 6. Very few points fall within the area of stability of tenorite (CuO(s)). On the diagram, point (3) corresponds to measured values in one of the Tienma-Qucun tombs. pH in these tombs is around 8, and measured Eh is around 175mV, although Wang does not seem to include details on measurement methods for Eh in her publication (Wang 2002).

Corrosion trajectories

The idea of corrosion trajectories was first raised by McNeil and Mohr (1993). On figure 6 a trajectory has been drawn showing what possibly may have happened to some Chinese bronzes. It starts at number (1), when the bronze was exposed to atmospheric conditions. It probably corroded some during use and then was buried -- again under atmospheric conditions. With rotting of organic material in the closed tomb, and (in some cases) large amounts of charcoal being included in the burial, the atmosphere will change from oxidizing to reducing. pH

will also rise due to decomposition products and large amounts of CO₂ in the surrounding earth. Corroding conditions will move from number (1) to number (3), or in some cases all the way down to number (2). The trajectory from (1) to (2) moves through areas of stability of malachite, cuprite, and pure copper, all with tin present as SnO₂. Initial corrosion (at point (1)) would yield malachite plus tin oxide, although if it were taking place in a situation where electrolytes were more dilute, copper could have been removed from the surface as a solution, perhaps leaving the delta phase behind. As conditions change, formation of cuprite will be favored. At even lower values of Eh, copper will be stable; the bronze can still corrode to form SnO₂, but copper from the corroding bronze may then redeposit as metallic copper. In fact, at these low values of Eh, the corrosion of the alpha phase in the bronze (similar to pure copper) will be suppressed and the higher tin phase (usually the delta) will be corroded preferentially. This is exactly the condition we see on most ancient Chinese bronzes. More studies of actual conditions in burials and correlation of these with actual corroded bronzes are needed. The new Eh-pH diagrams give a framework for investigations to proceed.

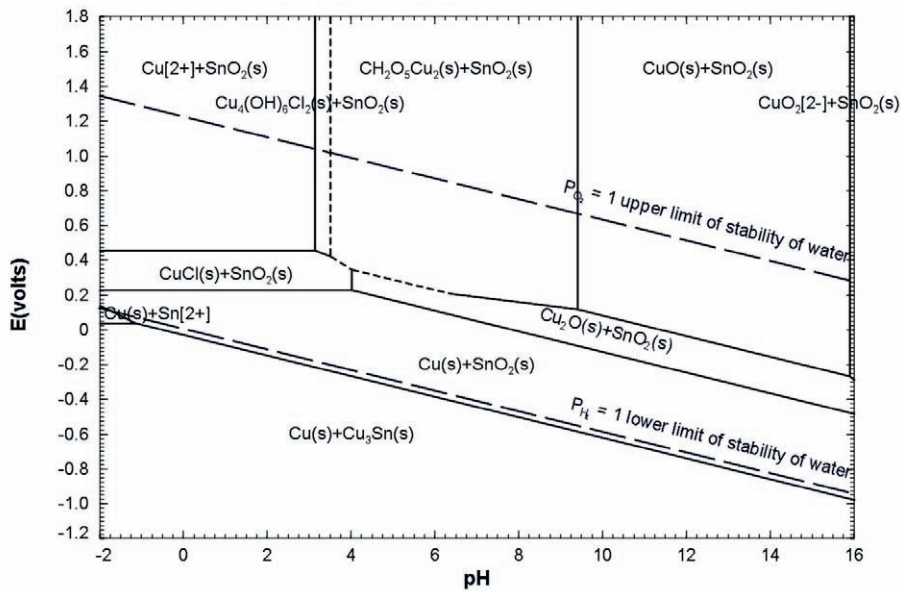


Figure 4: Eh-pH diagram for the Cu-Sn-Cl- CO_2 - H_2O system at 298.15 K. $\log_{10} m(\text{Cl}^-) = -2$ (355 ppm), $\log_{10} m(\text{CO}_2) = 0$ (4.4%); $\log_{10} m$ for other aqueous species = 1.

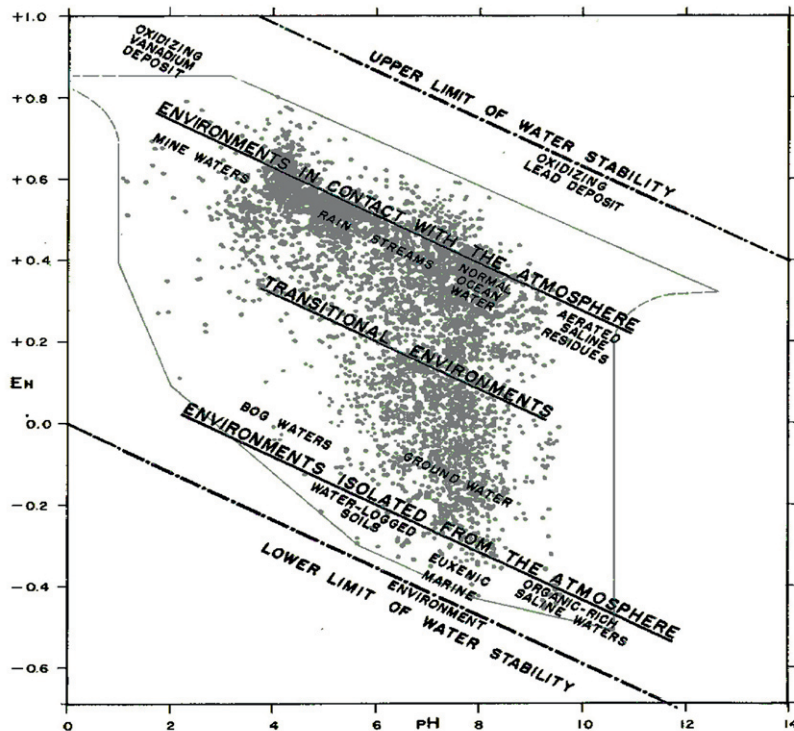


Figure 5: Environments represented on the Eh-pH diagram with the point cloud of actual measured Eh-pH values for thousands of environments (Garrels and Christ 1965)

Redeposited copper

Much work has been done on the question of redeposited copper or free copper (See, inter alia, Wang 2002; Bosi et al. 2002; Wang et al. 2006). From looking at these Eh-pH diagrams, it seems clear that copper will redeposit at low Eh values. Many of the various morphologies shown by free copper in archaeological bronzes are simply due to the fact that decuprification of some phase of the alloy, often delta, is followed by redeposition of the copper in whatever cavities are present. The process can reverse if conditions change.

Initial corrosion of bronzes

Much work has also been done on the questions of the initial corrosion on coppers and bronzes, marker layers showing the original surface (Bertholon 2001), how this initial corrosion grows to archaeological thickness, and what conditions lead to desirable patinas or disfiguring corrosion crusts. The idea of decuprification and formation of a tin oxide layer through which copper ions can migrate, giving rise to smooth "Type-I" patinas (Robbiola and Fiaud 1998) is well supported by the evidence. What we have seen on the Eh-pH diagrams about tin

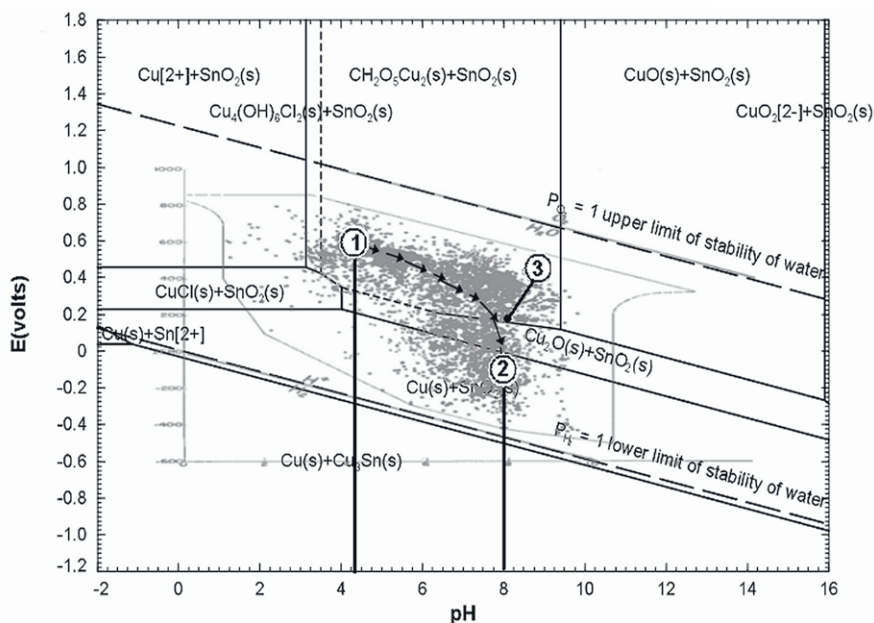


Figure 6: Eh-pH diagram for the Cu-Sn-Cl- CO₂-H₂O system at 298.15°K. Log₁₀ m(Cl⁻) = -2 (355 ppm), log₁₀ m(CO₂) = 0 (4.4%); log₁₀ m for other aqueous species = 1. The point cloud of environments from Figure 6 is superimposed, vertical lines at pH 4.3 and 8.0 added, and a possible corrosion trajectory drawn in. Point (1): beginning of corrosion; point (2): possible conditions in a deep tomb in China; point (3): actual measured conditions in Tienma-Qucun Tomb M93 (Wang 2002)

oxide does not contradict this idea. A recent study of corrosion of a 13% (by weight) tin bronze in stagnant aerated 0.5 M NaCl solution (Debiemme-Chouvy et al. 2001) showed that the surface was initially covered with a thin SnO₂ layer. At the beginning of immersion, thickness of the initial SnO₂ layer increases due to selective copper dissolution. Then it gets progressively buried beneath a Cu₂O film.

Debiemme-Chouvy et. al. took care to homogenize the 13% tin bronze very carefully. Their micrographs, however, show differences in the copper and tin concentrations of areas on the corroded surface. Archaeological bronzes present a great variety of surface conditions (see figure 7, showing metallographic structures of alloys similar to those used for Chinese mirrors, and Taube et al. in press). Studying initial oxide formation on surfaces with different metallographic structures would form a very interesting experiment.

Anything that disturbs initial corrosion films or the longer-term films formed during archaeological burial will set off corrosion.

When the bronzes are removed from a stable environment to other environmental conditions, corrosion can be severe -- not only bronze disease and chloridic corrosion, but also corrosion at cracks and surface damages.

Conclusion

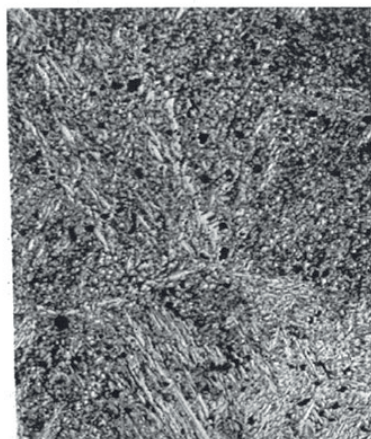
The construction of Eh-pH diagrams using copper and tin together, as well as intermetallic phases, has yielded greater insight into corrosion processes. The diagrams can also lead to further testable hypotheses about bronze corrosion and, one hopes, improved conservation methods in the future.

Acknowledgements

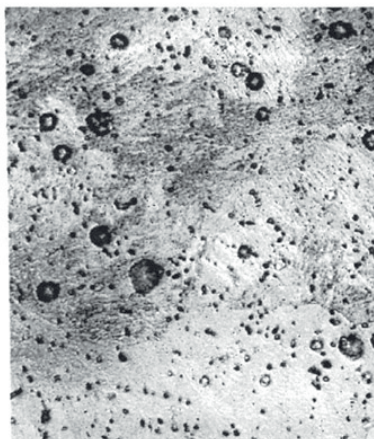
This program was undertaken with the financial support of the Rubin-Ladd Foundation and of the Department of Conservation and Scientific Research, Freer Gallery of Art and Arthur M. Sackler Gallery, Smithsonian Institution. Much helpful assistance was rendered from the Library of Lehigh University.

References

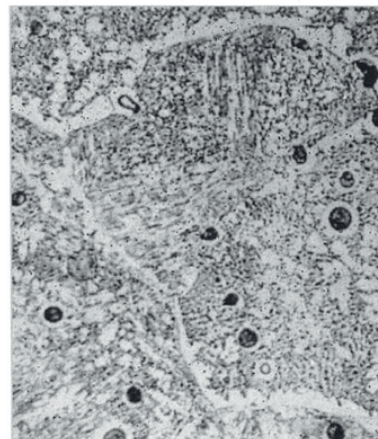
- Bale C.W., P. Chartrand, S.A. Deckerov, G. Eriksson, K. Hack, R. Ben Mahfoud, J. Melançon, A.D. Pelton and S. Petersen. 2002. FactSage Thermochemical Software and Databases, Calphad Journal, 62, 189-228
- Bertholon R. 2001. The Original Surface of Corroded Metallic Archaeological Objects: Characterization and Location, La Revue De Métallurgie-CIT/Science Et Génie Des Matériaux, no. 9, 817-823
- Bosi C., G.L. Garagnani, V. Imbeni, C. Martini, R. Mazzeo and G. Poli. 2002. Unalloyed Copper Inclusions in Ancient Bronze Artifacts, Journal of Materials Science, 37, 4285-4298
- Chase W.T. 1994. Chinese Bronzes: Casting, Finishing, Patination, and Corrosion, in Ancient and Historic Metals: Conservation and Scientific Research, eds. David A. Scott, Jerry Podany, and Brian B. Consadine. Marina del Rey, CA: J. Paul Getty Museum and the Getty Conservation Institute, 85-118
- Debiemme-Chouvy C., F. Ammeloot and E.M.M. Sutter. 2001. X-Ray Photoemission Investigation of the Corrosion Film Formed on a Polished Cu-13Sn Alloy in Aerated NaCl Solution, Applied Surface Science, 174, no.1, 55-61
- Garrels, R.M. and C.L. Christ. 1965. Solutions, Minerals, and Equilibria, New York: Harper and Row
- Lins A, and T. Power. 1994. The Corrosion of Bronze Monuments in Polluted Urban Sites: a Report on the Stability of Copper Mineral Species at Different pH Levels, in Ancient and Historic Metals: Conservation and Scientific Research, eds. David A. Scott, Jerry Podany, and Brian B. Consadine. Marina del Rey, CA: J. Paul Getty Museum and the Getty Conservation Institute, 119-152
- McNeil M.B. and D.W. Mohr. 1993. Formation of Copper-Iron Sulfide Minerals During Corrosion of Artifacts and Possible Imple-



73-24-3 (alpha and delta) plus alpha
(actually 24.7% tin)



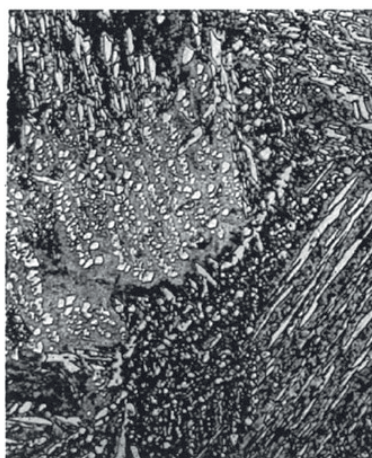
72-25-3 alpha plus delta
(actually 25.8% tin)



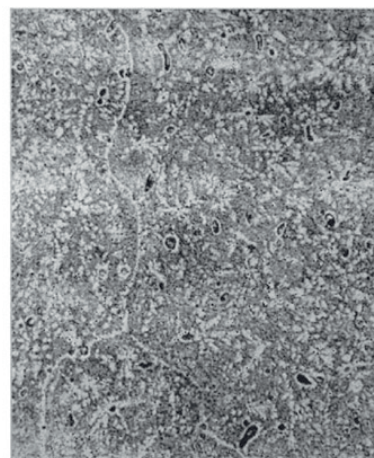
71-26-3 delta plus (alpha + Delta)
(actually 26.8% tin)



75-22-3 alpha plus (alpha and delta)
(actually 22.7% tin)



76-23 alpha plus (alpha and delta)
(no lead)



71-26-3 delta plus (alpha and delta)
Low magnification

Figure 7: Copper-tin alloys with around 25% weight percent of tin (all with 3% lead except as noted). The alloy with 25.8% tin (top center) has an extremely fine structure (Chase 1994). Width of photographic field for all views except that on the lower right = 0.27 mm; lower right = 0.54 mm

cations for Pseudogilding, *Geoarchaeology: An International Journal*, 8, no.1, 23-33

- Pelton, A.D., C.W. Bale and W.T. Thompson. 1977. F*A*C*T - a Computerized Canadian Thermodynamic Data Treatment Centre, Proceedings of Applications of Phase Diagrams in Metallurgy and Ceramics Gaithersburg, Maryland: NIST
- Pourbaix, M. 1977. Electrochemical Corrosion and Reduction, *Corrosion and Metal Artifacts - A Dialogue Between Conservators and Archaeologists and Corrosion Scientists*, eds. B. Floyd Brown, Harry C. Burnett, W. Thomas Chase, Martha Goodway, Jerome Kruger, and Marcel Pourbaix. NBS Special Publication, no. 479. Washington, D.C.: National Bureau of Standards, 1-16
- Robbiola L., J.M. Blengino and C. Fiaud. 1998. Morphology and Mechanisms of Formation of Natural Patinas on Archaeological Cu-Sn Alloys, *Corrosion Science*, 40, no.12, 2083-2111
- Schweizer F. 1994. Bronze Objects From Lake Sites: From Patina to "Biography", in *Ancient and Historic Metals: Conservation and Scientific Research*, eds. David A. Scott, Jerry Podany, and Brian B. Considine. Marina del Rey, CA: J. Paul Getty Museum and the Getty Conservation Institute, 33-50
- Scott D.A. 2002. *Copper and Bronze in Art*, Los Angeles: The Getty Conservation Institute
- Taube M., A.H. King and W.T. Chase. In press. Transformation of Ancient Chinese Two-Phase Bronze Surfaces to Smooth Adherent Patinas, *Phase Transitions*
- Wang D. 1997. In-Situ Oxidation Study of Cu, Sn, and Cu-Sn Intermetallics At Low Temperatures By X-Ray Photoelectron Spectroscopy, Doctoral Dissertation, Lehigh University
- Wang J., X. Chunchun, and L. Guocheng. 2006. Formation Processes of CuCl and Regenerated Copper Crystals on Bronze Surfaces in Neutral and Acidic Media, *Applied Surface Science*, 252, no.18, 6294-6303
- Wang Q. 2002. Metalworking Technology and Deterioration of Jin Bronzes From the Tianma-Qucun Site, Shanxi, China, BAR International Series 1023. Oxford: Archaeopress